Suspension of deformable particles in Newtonian and viscoelastic fluids in a microchannel

Amir Hossein Raffiee · Sadegh Dabiri · Arezoo M. Ardekani

Abstract In this paper, we study a suspension of cells at a moderate volume fraction flowing in a microchannel filled with Newtonian or viscoelastic fluids and investigate the role of cell size, cell volume fraction, inertia, deformability and fluid elasticity on the cell distribution. Our results suggest that the use of constant-viscosity viscoelastic fluid pushes the cells toward the channel centerline which can be used in microfluidic devices used for cell focusing such as cytometers. The cell-free layer increases which provides larger gap for separating rare cells in microfluidic devices. Furthermore, we show that the volumetric flow rate can be significantly enhanced with the addition of polymers in the suspending fluid. This effect enhances the processing speed which is of interest in designing microfluidic devices. This fundamental study can provide insight on the role of rheological properties of the fluid that can be tuned to control the motion of the cells for efficient design of microfluidic devices.

Keywords Cell migration in polymeric fluids · Cell focusing · Elasto-inertial cell migration

Amir Hossein Raffiee
School of Mechanical Engineering, Purdue University, West Lafayette, IN 47907, USA

Sadegh Dabiri
Department of Agricultural and Biological Engineering, Purdue University, West Lafayette, IN 47907, USA
School of Mechanical Engineering, Purdue University, West Lafayette, IN 47907, USA

Arezoo M. Ardekani
School of Mechanical Engineering, Purdue University, West Lafayette, IN 47907, USA

1 Introduction

The motion of synthetic capsules and living cells in microchannels has been the subject of numerous studies in the last decade due to its significance in engineering and biomedical applications [7, 43, 44]. Cell sorting and separation are common processes that are used for various purposes such as separation of leukocytes from blood used in DNA sequencing [21]. Early diagnosis of lethal diseases such as cancer [58] can be conducted by isolation of rare cells in blood, which is a complex suspension of cells. Furthermore, fractionated healthy blood components are used for different therapeutic applications such as platelet transfusion [54]. Cell isolation and enrichment provide a better platform to biologists to study and analyze various properties of living cells [21, 25]. In this regard, microfluidic devices provide a platform to achieve aforementioned needs while overcoming challenges such as sample contamination, cost and complexity of the procedures [40]. Besides, these devices offer higher accuracy for analysis and increased automation of the process [6, 20]. Accordingly, there is a high demand for developing techniques to precisely control trajectories of cells and manipulate them in a desired manner. Some of the proposed techniques employ external factors such as electric [42], magnetic [41] and acoustic [19] fields and sheath flows [23, 30, 56]. Even though they can offer high throughput sample processing, the complexity of the procedure and high cost limit their utilization in clinical applications [21]. Furthermore, these methods require cell manipulation that may change biological properties of the cells [11]. Hence, there is a growing interest in employing label-free techniques that take advantage of physical properties of the cells such as size, shape and deformability to control their trajectories in microfluidic devices

[11, 21, 40]. Inertial microfluidics are among the proposed techniques that use inertial forces to induce cell migration in microchannels [4, 13, 14]. In this technique, cells focus at an equilibrium position depending on their physical properties [12, 24, 29]. The particles flowing in a Newtonian fluid follow the streamlines without any transversal migration for low Reynolds numbers [22]. With increasing the Reynolds number the inertial force becomes important and the cross-streamline migration of particles is observed [31, 33]. In this case, the particle experiences two opposing forces: (i) shear-gradient induced force that pushes the particle toward the wall [1] and (ii) the wall-induced repulsive force that drives it toward the channel center [61]. The balance between these two forces determines the equilibrium position of the flowing particle in the channel cross-section [34]. This phenomenon was first observed by Segré and Silberberg [52]. In their experiments, randomly distributed particles at tube inlet assembled at an annulus with radius of 0.6 times the radius of the tube. This result was later confirmed numerically [18], analytically [51] and experimentally [26]. Previous investigations show that the deformability of the cell can affect its trajectory in the microchannel [27, 47, 50]. Due to deformability of cell membrane, a deformability-induced force is generated and the interplay of all the above forces governs the equilibrium position of the flowing cells [47]. In our previous work [47], we studied the effect of cell deformability on the equilibrium position of a single deformable cell. Our results show that deformability-induced force drives the cells toward the channel centerline in a Newtonian fluid. Recent studies on microfluidic devices introduced an alternative way for cell focusing by adding a polymer to the suspending fluid [8, 16, 38]. In this method, the polymer chains in the fluid are stretched and generate an uneven normal stress on the flowing particles. This phenomenon leads to a net elastic force that interacts with the inertial force and affects the migration dynamics and equilibrium position of the particle [10, 11]. This phenomenon has been experimentally and analytically [9, 33, 34, 60] observed. The particle migration depends on the fluid rheology, cell size, channel geometry and volumetric flow rate [34, 59]. There are several experimental studies that showed promising results for cell separation and focusing using polymeric fluid as the suspending fluid. Lim *et al.* [36] used hyaluronic acid (HA) in the suspending fluid and successfully focused solid particles and leukocytes at the channel center. Furthermore, the same method was used to separate human breast carcinoma and leukocyte cells in a straight microchannel [39] which highlights the effect of cell size and deformability on the particle migration flowing in a viscoelastic polymeric fluid. The effect of size and deformability was also observed in Liu *et al.* [37], where solid particles, living cells and bacteria were separated by focusing in different locations in the channel cross-section. Previous studies [33, 47, 49, 53] show that fluid rheological properties are important on the dynamics of cell migration in microchannels. In our previous work [47], we have shown that a constant-viscosity viscoelastic fluid drives the particle toward the channel centerline, while a shear-thinning viscoelastic fluid exhibits an opposite behavior. The equilibrium position of cell depends on the cell size, deformability and volumetric flow rate. Our previous results for a single cell migration agree well with previous experimental and numerical studies in dilute suspensions [34, 59].

Despite the importance of the dynamics of cell suspensions in a microchannel, previous experimental and computational studies focus on the migration of cells in a dilute regime. This limitation prevents us to evaluate the performance of the developed techniques for rich samples such as blood which has higher cell concentrations. The optical techniques cannot be effectively used for quantification of samples at high cell concentrations. In order to overcome this limitation, we focus on a suspension of deformable cells in Newtonian and polymeric fluids in semidilute and concentrated regimes and investigate the role of various factors including cell size, deformability, inertia and viscoelasticity of the suspending fluid. Our results provide fundamental understanding of the dynamics of suspension of cells in a straight microchannel used in various microfluidic devices.

2 Methodology

2.1 Governing equations

Dynamics of the deformable cells flowing in microchannel is governed by the momentum and continuity equations. In this study, we assume that the inner fluid of the cell and suspending fluid are incompressible. Therefore, we have:

$$\nabla.\mathbf{u} = 0, \tag{1}$$

$$\frac{\partial(\rho\mathbf{u})}{\partial t} + \nabla.(\rho\mathbf{u}\mathbf{u}) = -\nabla p + \nabla.\boldsymbol{\tau} + \mathbf{F}. \tag{2}$$

Here, ρ is the density of the fluid, t denotes the time, $\mathbf{u}$ is the velocity vector and p and $\boldsymbol{\tau}$ represent pressure and stress tensor, respectively. The stress tensor in a Newtonian fluid is a function of fluid viscosity μ and strain rate tensor $\mathbf{D} = \nabla\mathbf{u} + \nabla\mathbf{u}^T$, where $\boldsymbol{\tau} = \mu\mathbf{D}$. We use a front-tracking [57] method to track the interface and capture the change in fluid properties across the

membrane. In this method, a single set of equations is solved in the entire computational domain. In equation 2, $\mathbf{F}$ represents the smoothed elastic force generated due to the deformation of cell membrane which can be obtained as:

$$\mathbf{F}(\mathbf{x},t) = \int_{\partial B} \boldsymbol{f}(\mathbf{x}_i,t)\delta(\mathbf{x}-\mathbf{x}_i)dV. \tag{3}$$

Here, $\boldsymbol{f}$ is the membrane resistive force exerted on the fluid. This force is zero everywhere in the domain except for the membrane interface. In equation 3, $\mathbf{x}$ and $\mathbf{x}_i$ denote an arbitrary point in the computational domain and a point on the cell membrane, respectively. Furthermore, δ and V are the Dirac delta function and volume, respectively. In order to distribute the resistive force on Eulerian grid points surrounding the membrane, a smoothed delta function is employed:

$$\delta(\mathbf{x}) = \tilde{D}(x)\tilde{D}(y)\tilde{D}(z), \tag{4}$$

$$\tilde{D}(x) = \frac{1}{4\Delta}(1+\cos(\frac{\pi}{2\Delta}x)), |x| \leq 2\Delta, \tag{5}$$

where Δ is the Eulerian grid size. In order to simulate the cell membrane we use the Skalak [55] model. Ramanujan *et al.* [48] showed that the Skalak model can capture the behaviour of deformable cells under various conditions and their results agreed well with experiments [2]. In this model, the cell is assumed to behave as a deformable capsule that has a resistance against shear deformation and area dilatation. Accordingly, a strain energy function is assigned to the membrane as follows:

$$W = \frac{E_s}{12}((\epsilon_1^2+\epsilon_2^2-2)^2 + 2(\epsilon_1^2+\epsilon_2^2-2) - 2(\epsilon_1^2\epsilon_2^2-1)) + \frac{E_a}{12}(\epsilon_1^2\epsilon_2^2-1)^2, \tag{6}$$

where E_s and E_a denote shear and dilatation moduli and ϵ_1 and ϵ_2 are principal strains. In this study, we consider $\frac{E_a}{E_s} = 2$ following Krüger *et al.* [28]. For the range of Reynolds and Laplace numbers used in this study, the area extension is less than 8%. We use a finite element method [3] to obtain the force $\boldsymbol{f}$ in equation 3. The validation of this model against previously published results is presented in our previous work [46]. The Navier Stokes equations are solved using a finite volume method. The time derivatives are discretized using an explicit Euler scheme and discretization for the convective and diffusive terms are conducted using Quadratic Upstream Interpolation for Convective Kinematics [32] (QUICK) and central difference schemes, respectively. The pressure-velocity coupling is conducted using a projection method [5].

In order to solve for a viscoelastic suspending fluid, the total stress $\boldsymbol{\tau}$ is split into two parts: (i) solvent stress tensor $\boldsymbol{\tau_s}$ and (ii) polymeric stress tensor $\boldsymbol{\tau_p}$ as follows:

$$\boldsymbol{\tau} = \boldsymbol{\tau_s} + \boldsymbol{\tau_p}. \tag{7}$$

Here, $\boldsymbol{\tau_s}$ can be written as:

$$\boldsymbol{\tau_s} = \mu_s \mathbf{D}, \tag{8}$$

where μ_s is the solvent viscosity. In this study, the Oldroyd-B constitutive equation is used to represent the stress tensor.

$$\lambda \overset{\triangledown}{\boldsymbol{\tau_p}} + \boldsymbol{\tau_p} = \mu_p \mathbf{D}, \tag{9}$$

In this equation, μ_p is the polymer viscosity and λ represents the fluid relaxation time. Equation 9 models a constant-viscosity viscoelastic fluid. Here, $\overset{\triangledown}{\boldsymbol{\tau_p}}$ is the upper convected time derivative defined as:

$$\overset{\triangledown}{\boldsymbol{\tau_p}} = \frac{\partial \boldsymbol{\tau_p}}{\partial t} + \mathbf{u}.\nabla\boldsymbol{\tau_p} - \nabla\mathbf{u}\boldsymbol{\tau_p} - \boldsymbol{\tau_p}\nabla\mathbf{u}^T, \tag{10}$$

The details of the numerical scheme used to solve equation 9 and its validation are explained in our previous work [46].

2.2 Problem setup

In this work, the computational domain is a straight squared channel illustrated in Fig. 1. The edge of the channel is $2W$ and the channel length is set to be $4W$. We applied a periodic boundary condition in x direction and a no-slip boundary condition is implemented in y and z directions. In this problem, W and U_0 (the undisturbed centerline velocity of the channel in the absence of capsules) are used as the characteristic length and velocity scales, respectively. Here in this work, dimensionless variables are defined as $t^* = \frac{tU_0}{W}$ (time), $\mathbf{x}^* = \frac{\mathbf{x}}{W}$ (position), $\mathbf{u}^* = \frac{\mathbf{u}}{U_0}$ (velocity) and $P^* = \frac{pW}{\mu U_0}$ (pressure). Hence, the dimensionless numbers governing the problem are: (i) the Reynolds number $Re = \frac{\rho U_0 2W}{\mu}$ that represents the ratio of inertial to the viscous forces, (ii) the Laplace number $La = \frac{2\rho E_s a}{\mu^2}$ denoting the deformability of the cell, (iii) ϕ that shows the volume fraction of cells in the microchannel, (iv) the Weissenberg number $Wi = \frac{\lambda U_0}{W}$ showing the ratio of elastic to viscous forces, (v) $\beta = \frac{\mu_p}{\mu}$ representing the ratio of the polymer viscosity to total viscosity ($\mu = \mu_s + \mu_p$) and finally (vi) the aspect ratio $AR = \frac{a}{W}$ that shows the blockage ratio in the microchannel. We assume that the inner fluid of the cells is a Newtonian fluid with a density and viscosity equal to those of the outer fluid ($(\mu_s+\mu_p)_{outer} = (\mu_s)_{inner}$ and $\rho_{inner} = \rho_{outer}$). Unless otherwise stated, β is set to 0.9 and the cells are

initially spherical. The computational domain and cell membrane are discretized using $128 \times 76 \times 76$ Eulerian grid points in x, y and z directions and 20000 Lagrangian grid points. The mesh and domain size independency tests are provided in the Appendix.

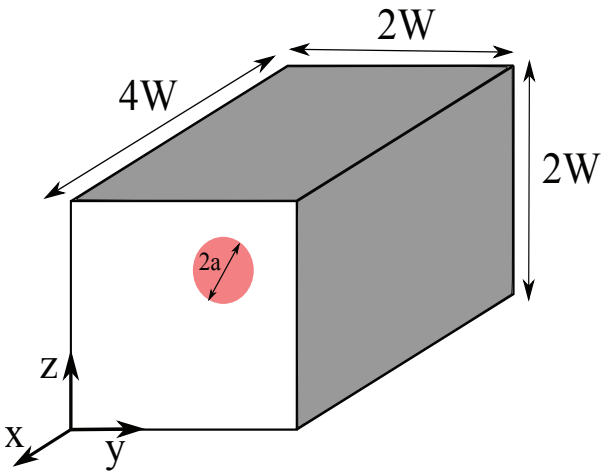

Fig. 1: Schematic of problem setup

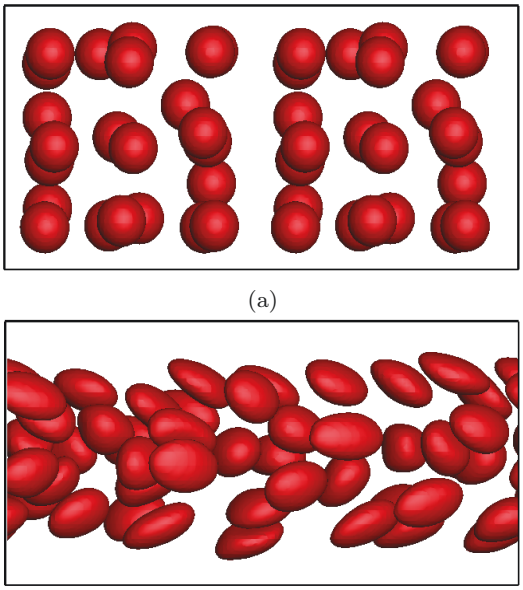

(a)

(b)

Fig. 2: The distribution of cells at (a) $t^* = 0$ and (b) at $t^* = 1336$ for $\phi = 10\%$, $\frac{a}{W} = 0.2$, $La = 1$ and $Re = 37.8$

3 Result and discussion

3.1 Newtonian fluid

In this section, the migration of cells flowing in a Newtonian fluid is investigated and the effects of various factors including deformability (La), cell volume fraction (ϕ), inertia (Re) and cell size ($\frac{a}{W}$) on cell distribution are explored. The computational domain is filled with a homogeneous suspension of randomly distributed cells (cells with the same size and deformability) along the channel. A constant pressure gradient is applied to generate a flow in the microchannel and cells flow and migrate across the microchannel due to cell-cell and cell-fluid interactions. The simulation is run long enough that the suspension reach a statistically steady state. The Reynolds number is set to 37.8 unless otherwise stated.

Figure 2 illustrates the cell suspension at two time instances $t^* = 0$ and $t^* = 1336$ for $La = 1$, $\phi = 10\%$ and $\frac{a}{W} = 0.2$. The cells interact and deform in the channel. Due to the low shear rate in the central region of the channel, cells maintain their initial spherical shape, while cell deformation is more significant as the cells get closer to the wall, where the shear rate is higher. Cells migrate in the cross-stream direction and accumulate near the center of the channel. This migration behavior toward the centerline is caused by the deformability-induced force acting on the cells. The interplay between this force, inertial lift force and wall-induced force determines the focal location of cells [27, 47, 50] in the microchannel. In addition to the above mentioned forces, the cell-cell interaction becomes important when we consider cell suspensions at a moderate volume fraction. The migration of cells toward the center can also be observed by comparing cell distribution at two different time instances in Fig. 2, where the accumulation of cells near the center of channel is significant. To study the motion of a suspension of cells, the ensemble average of cell distance from the centerline $\langle r^* \rangle$ is computed. Figure 3 shows the temporal evolution of average distance of cells from the channel centerline for various La number at $\phi = 10\%$, $\frac{a}{W} = 0.3$. According to this figure, $\langle r^* \rangle$ initially decreases and reaches a quasi-steady state. The initial decrease in $\langle r^* \rangle$ shows the net migration of cells toward the centerline due to the deformability-induced force acting on the cells. The steady value of cell position is computed by temporally averaging $\langle r^* \rangle$ over the time period during which statistically steady state is reached (see Fig. 4 for $Re = 37.8$). The cell distance from centerline increases with increasing La number (decreasing deformability) which is in agreement with the behavior of a single cell in a microchannel [27, 47, 50]. This change is attributed to the effect of La number on the deformability-induced force. As La increases this force gets weaker and the inertial and wall-induced forces become dominant fac-

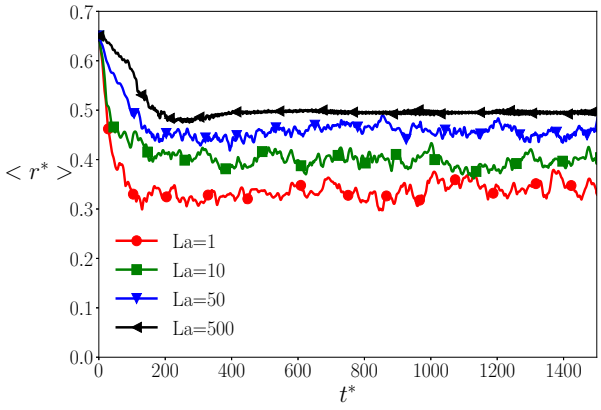

Fig. 3: Average cell distance from the centerline for $\phi = 10\%$, $\frac{a}{W} = 0.3$ and $Re = 37.8$

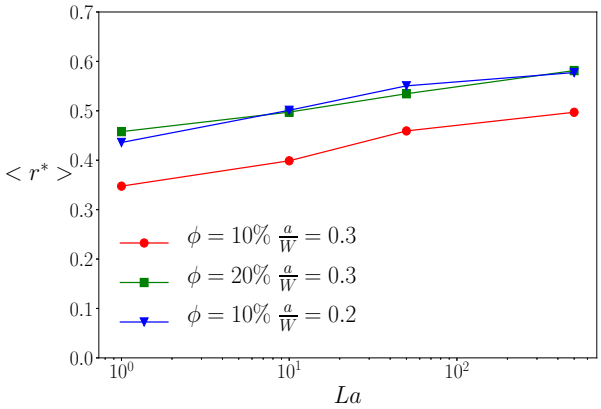

Fig. 4: Quasi-steady cell distance from the centerline for various La at $Re = 37.8$

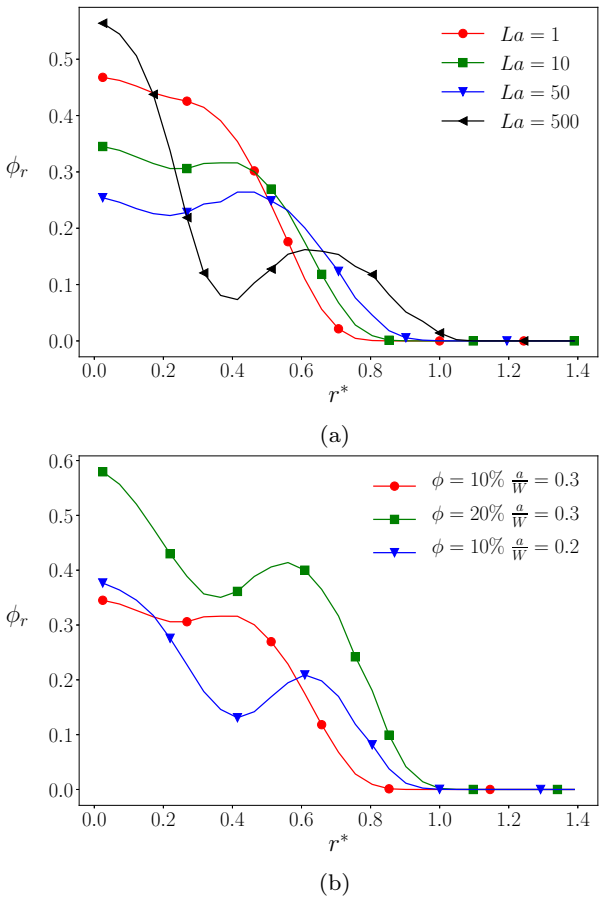

Fig. 5: Radial volume fraction for (a) $\phi = 10\%$, $\frac{a}{W} = 0.3$ and $Re = 37.8$ and (b) for $La = 500$ and $Re = 37.8$

tors. Hence, the location of cells with a high Laplace number is close to that of solid particle flowing in a microchannel. Figure 4 also exhibits that increasing the cell volume fraction leads to increase in the cell distance from the channel centerline. This behavior is due to the increase in the cell-cell interaction as the number of cells flowing in the channel increases. Furthermore, the cell size has an important role on the net motion of cells. Comparing the average distance for different blockage ratios ($\frac{a}{W} = 0.2$ and 0.3) indicates that bigger cells get closer to the centerline. According to Schaaf *et al.* [50], the deformability-induced forces scale proportionally with the size of the cells. Hence, bigger cells experience a larger force towards the centerline. In order to study the quasi-steady distribution of cells in a microchannel, two quantities including radial volume fraction (ϕ_r) and local volume fraction (ϕ_l) are defined. The local volume fraction represents the cell distribution across the microchannel and is defined as the fraction of volume $\Delta y \Delta z L_x$ (L_x is the channel length in x direction) occupied by the cells at different y and z across the channel cross-section. To find ϕ_r, eq. 11 is introduced.

$$\phi_r = \frac{1}{A_{r,r+\Delta r}} \int_r^{r+\Delta r} \phi_l 2\pi r dr, \tag{11}$$

In this equation, r is the distance from the channel centerline and $A_{r,r+\Delta r}$ is the area between r and $r + \Delta r$. Hence, the radial volume fraction (ϕ_r) is the fraction of microchannel volume between r and $r + \Delta r$ that is occupied by cells. The radial volume fraction for $\phi = 10\%$, $\frac{a}{W} = 0.3$ is plotted for various Laplace number in Fig. 5(a). According to this figure, the cells are not evenly distributed across the channel. The results show that the radial volume fraction of cells decreases with the distance from the channel centerline and it reaches to zero at a particular radius. The region in the microchannel in which the radial volume fraction is zero is called cell-free layer (CFL). The formation of this layer has been numerically and experimentally observed in previous studies [45, 62]. Furthermore, the same phenomenon occurs in blood vessels where the concentration of the red blood cells close to the vessel wall is far

less than its value in the core region [17]. The thickness of this layer is an important factor in designing microfluidic devices as it specifies the gap between the wall and suspending cells in the sample, where the rare cells should fall into to easier get separated. One of the important factors affecting the thickness of CFL is La number. The thickness of CFL increases with decreasing La number (Fig. 5(a)). The reason for this behavior is the tendency of deformable cells to migrate toward the core region and this tendency is enhanced by decreasing La number. Hence, the concentration of cells is higher in the central region leading to a thicker cell-depleted layer near the wall. The maximum radial volume fraction of cells at $La = 1$ occurs at the centerline and it decreases monotonously with the distance. The occurrence of the peak at the centerline is caused by two factors: (i) cell migration toward the centerline that yields to a significant cell accumulation in that region and (ii) the small area of the region ($A_{r,r+\Delta r}$) over which the radial volume fraction is computed in the central region. As the Laplace number increases an off-center peak in the radial volume fraction occurs, although the maximum radial volume fraction still occurs at the centerline due to the aforementioned reasons. In order to better understand this trend in cell distribution, the effect of deformability on the focal position of cells should be considered. Increasing the La number pushes the focal position of cells toward the wall of a microchannel [47, 50]. Therefore, a significant increase in the local volume fraction of cells is observed at off-center locations in the cross-section. This rise in the local volume fraction leads to the second peak in the radial volume fraction in Fig. 5(a). The effect of the cell volume fraction (ϕ) and the cell size on the cell distribution is plotted in Fig. 5(b). The thickness of CFL decreases with ϕ due to the increase in the number of cells and their interaction. Hence, the cells are more spread across the channel cross-section leading to a decrease in CFL thickness. Furthermore, decrease in the cell size results in decrease in the CFL thickness. This effect is attributed to the role of the cell size on the equilibrium position of cells shown in Fig. 4. The formation of the second peak is also observed for all the cases shown in Fig. 5(b). In order to elaborate the formation of the second peak in the radial volume fraction in details, the local volume fraction of cells (ϕ_l) in the channel cross-section at $\phi = 20\%$, $La = 10$ and $\frac{a}{W} = 0.3$ is plotted in Fig. 6. The blue region near the channel wall with zero concentration of cells is the cell free layer. According to this figure, ϕ_l has its maximum values at the center and at off-center locations shown by red regions. The off-center red regions in the channel cross-section lead to the formation of the second peak in

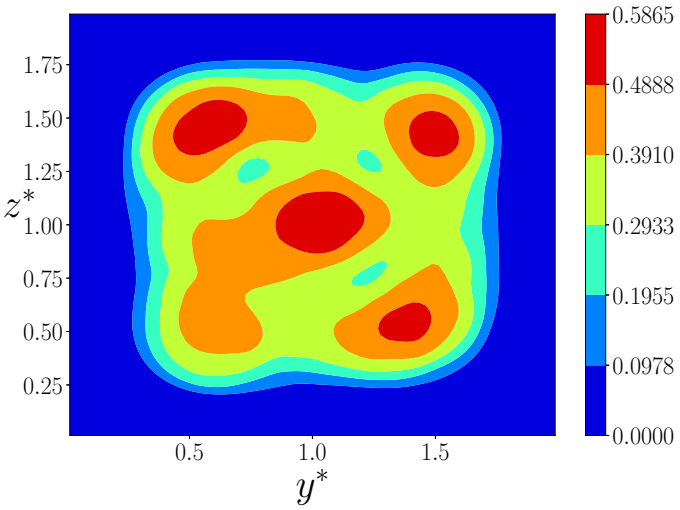

Fig. 6: Local volume fraction of cells at $\phi = 20\%$, $La = 10$, $\frac{a}{W} = 0.3$ and $Re = 37.8$

radial volume fraction (ϕ_r) in Fig. 5. This phenomenon is also observed in previous studies [35, 45] in which suspension of droplets and capsules were studied.

One of the important factors in evaluating the performance of microfluidic devices is the sample throughput. Hence, we plot the dimensionless volumetric flow rate of the suspension exiting the microchannel (Q^*) for various Laplace numbers in Fig. 7. Our results show

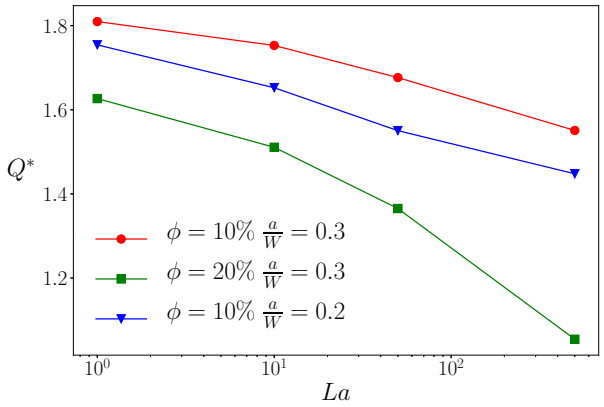

Fig. 7: The volumetric flow rate of the suspension for various La, ϕ and size at $Re = 37.8$

that the volumetric flow rate deceases with increasing Laplace number. This effect can be elaborated by considering the single cell dynamics in a microchannel. According to our previous study [47], a single cell flowing in the microchannel lags the surrounding fluid and its velocity is smaller than the local velocity of the fluid in the absence of the cell. This effect becomes more significant as the Laplace increases. Hence, the reduction of

volumetric flow rate with increase in La is expected. In order to quantify the effect of the cell deformability on the flow field, the velocity profile in the cross-section of microchannel is plotted for various La in Fig. 8. Our results show that decreasing the cell deformability results in decrease in the velocity across the cross-section. Furthermore, the velocity profiles for various La numbers are identical in the cell depleted region, while they are different in the regions occupied by the flowing cells. Figure 7 shows that the volumetric flow rate is also influenced by the cell volume fraction (ϕ) and the cell size. Accordingly, the reduction in the volumetric flow rate is observed with increasing the volume fraction (ϕ), while increasing the cell size ($\frac{a}{W}$) enhances Q^*. Here, we also study the effect of Reynolds number on the cell migration in the microchannel. In this work, we simulate the motion of cells at $\phi = 10\%$, $La = 500$ and two different cell sizes ($\frac{a}{W} = 0.2$ and 0.3) for various Re numbers. The average distance of the cells ($\langle r^* \rangle$) is plotted in Fig. 9. Our result shows that the average cell distance is not influenced by Reynolds number. This behavior is in agreement with previous studies [34, 47] that investigated the dynamics of a solid particle and a deformable capsule with high La number in a microchannel. Furthermore, the radial volume fraction distribution (ϕ_r) for the cell suspension with $\frac{a}{W} = 0.2$ is plotted in Fig. 10. This result also emphasizes that the steady spatial distribution of flowing cells is not affected by the Reynolds number and the change in the CFL thickness is negligible.

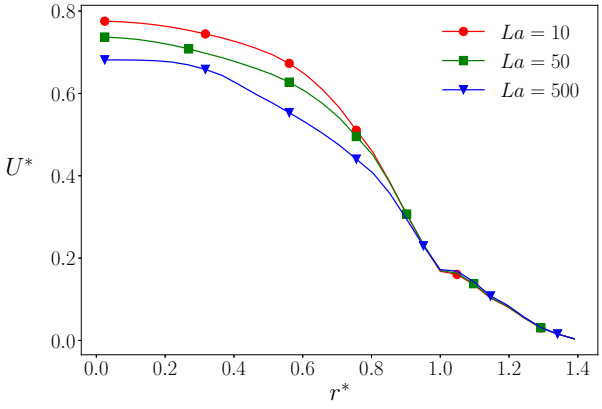

Fig. 8: The velocity profile in the microchannel at $\phi = 10\%$, $\frac{a}{W} = 0.3$ and $Re = 37.8$

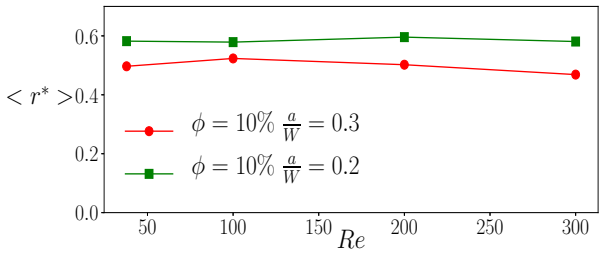

Fig. 9: Average cell distance for $\phi = 10\%$, $La = 500$ and $\frac{a}{W} = 0.2$ and 0.3

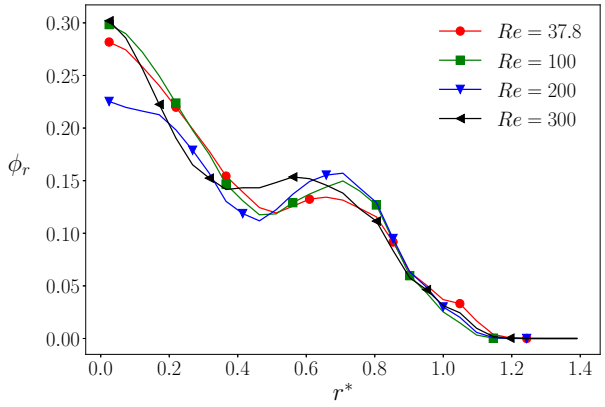

Fig. 10: Radial volume fraction distribution for $\phi = 10\%$, $La = 500$ and $\frac{a}{W} = 0.2$

3.2 Viscoelastic fluid

In this section, the effect of the polymeric fluid on the cell migration behavior is investigated. As it is mentioned in section 3.1, the migration of the cells is governed by the interplay between inertial lift force, deformability induced force, wall-induced force and cell-cell interaction. However, the cells flowing in a polymeric fluid experience an elastic force in addition to other forces. The elastic force is generated due to the deformation of polymer chains in the channel flow. The interplay between various forces determines the cell distribution in the channel. The motion and consequently the quasi-steady distance of cells suspended in a polymeric fluid is significantly influenced by the fluid elasticity.

Figure 11 plots the temporal evolution of the average cell distance from the channel centerline at $\phi = 10\%$, $La = 500$ and $\frac{a}{W} = 0.3$ for various Wi numbers ($Wi = 0$ corresponds to a Newtonian fluid). Our results show that the cell distance decreases as Wi number increases. Therefore, a constant-viscosity viscoelastic fluid pushes the cells toward the channel centerline. This behavior is in agreement with previous numerical and experimental studies [34, 36, 47] for an isolated

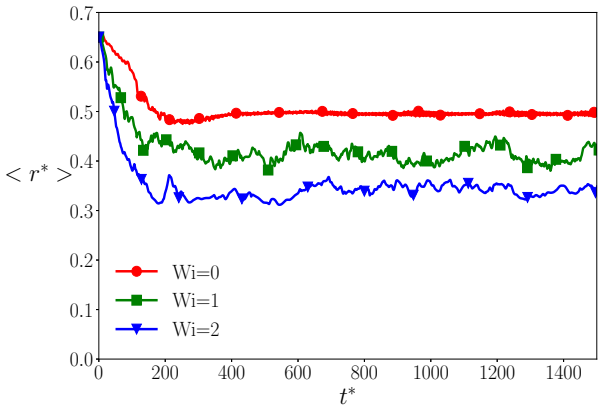

Fig. 11: Temporal evolution of cell distance from the centerline for $\phi = 10\%$, $\frac{a}{W} = 0.3$, $La = 500$ and $Re = 37.8$

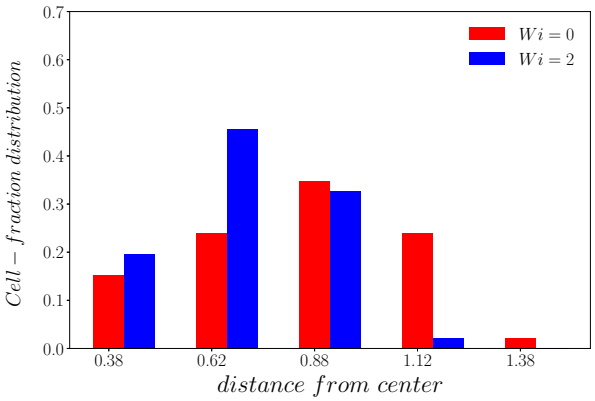

Fig. 12: Cell-fraction distribution of cells with $\frac{a}{W} = 0.2$, $La = 500$ and $\phi = 10\%$ with $Wi = 0$ and 2

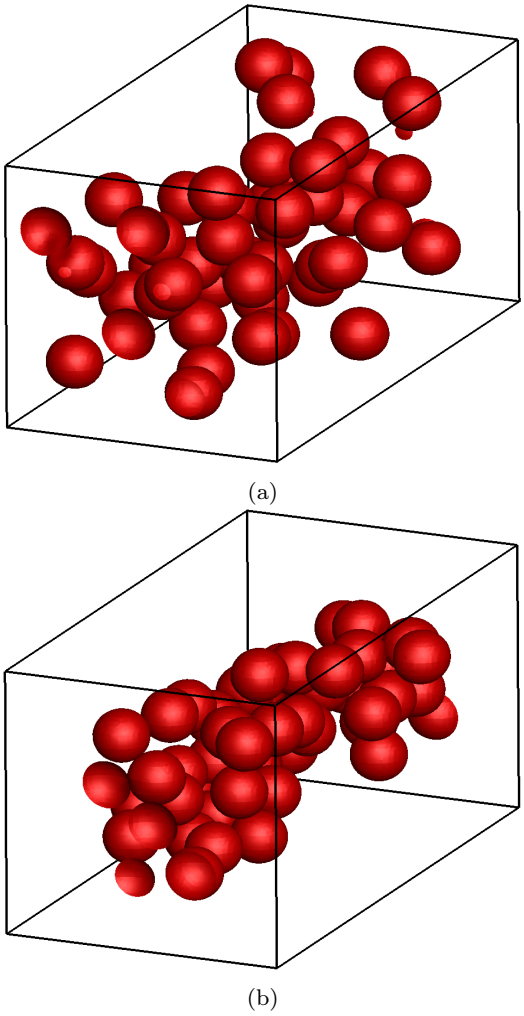

(a)

(b)

Fig. 13: The distribution of cells at $\phi = 10\%$, $La = 500$, $Re = 37.8$, $\frac{a}{W} = 0.2$ and (a) $Wi = 0$ and (b) $Wi = 2$

cell. This result suggests that the polymeric fluid can be used as a passive method in devices in which the main goal is cell focusing at the centerline such as cytometers. Furthermore, this method adds another variable to be tuned by the user to control the focal position of the cells in microfluidic devices. According to the results, the deformability-induced force and elastic force have reinforcing effect that drives the cells toward the centerline, while the inertial force has the opposite effect that pushes the cells toward the channel wall. Therefore, for a low Wi number, the inertial force is dominant and the resulting average cell distance is close to that of cells flowing in a Newtonian fluid, while for a high Wi number the elastic force has a significant effect and the cells accumulate in the centerline. In order to observe the effect of the polymeric fluid, the cell-fraction distribution of the cells with $\frac{a}{W} = 0.2$, $La = 500$ and $\phi = 10\%$ is plotted in Fig. 12. This figure shows the extent to which the cells are distributed across the microchannel. The fraction of cells located close to the centerline increases and the fraction of the cells close to the wall decreases significantly with increasing the Wi number. The cell fraction at $r^* = 1.38$ and 1.12 reaches nearly to zero. Furthermore, the location at which the maximum cell fraction occurs approaches to the centerline when polymers are added to the flowing fluid. The polymeric effect is also exhibited in Fig. 13, which shows the cell configuration for $\phi = 10\%$, $La = 500$ and $\frac{a}{W} = 0.2$ for two different values of Weissenberg number ($Wi = 0$ and 2). According to this figure, the cells flowing in a constant-viscosity viscoelastic fluid (Fig. 13(b)) focus more in the centerline compared to the cells flowing in a Newtonian fluid (Fig. 13(a)). In order to quantify the effect of polymeric fluid, the quasi-steady value of the average cell distance ($\langle r^* \rangle$) for various cell sizes and volume fractions is plotted as a function of Wi number in Fig. 14. The cell distance from the centerline decreases with increase in Wi number for various ϕ and $\frac{a}{W}$. The

decrease in $\langle r^* \rangle$ continues until the Wi number reaches a critical value above which the cell distance does not reduce further and reaches a plateau. This behavior is attributed to the cell-cell interaction that has an opposing effect against elastic effect and does not allow the cells to focus at the centerline. In other words, the cells are accumulated in the core region and the distance between the cells cannot be further reduced. This effect can be seen in Fig. 13 (b) that illustrates the distribution of cells in the central region. As it is shown in Fig. 14, the cell distance is not computed for Wi above 2 for two cases ($\phi = 20\%$, $\frac{a}{W} = 0.3$ and $\phi = 10\%$, $\frac{a}{W} = 0.2$). The lack of data for these cases is due to the numerical instability occurring for larger Wi numbers and volume fractions. The effect of the cell volume fraction (ϕ) and the cell size ($\frac{a}{W}$) is similar to their effect in a Newtonian fluid. Increasing the volume fraction increases the cell distance and increasing the cell size decreases the cell distance from the centerline. In order

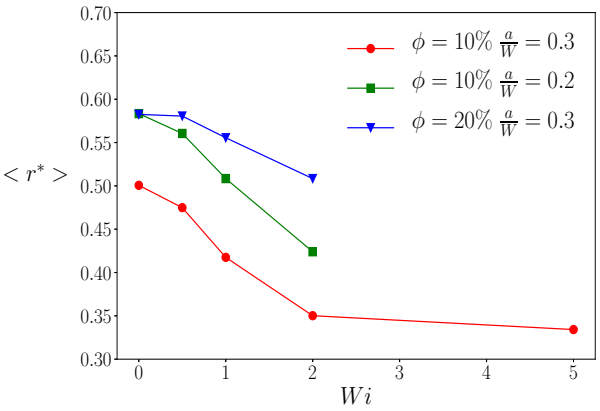

Fig. 14: Quasi-steady cell distance from the centerline for various Wi numbers at $Re = 37.8$

to study the effect of elasticity on CFL thickness, the radial volume fraction is plotted in Fig. 15 for $\phi = 10\%$, $\frac{a}{W} = 0.3$ and $Re = 37.8$. The thickness of the CFL increases with increasing Wi number. This change is attributed to the polymer chains driving the cells more effectively toward the centerline with increasing Wi number. Hence, a larger region in the vicinity of channel walls remain depleted from the cells. Furthermore, the location of the off-center peak in the radial volume fraction of the cells approaches to the centerline as the elasticity of the suspending fluid increases which is also due to the enhanced tendency of the cells in accumulating in the core region. The effect of the polymeric fluid on the throughput of microfluidic devices is also studied in this section. The volumetric flow rate of the exiting suspension is measured under various Wi numbers and

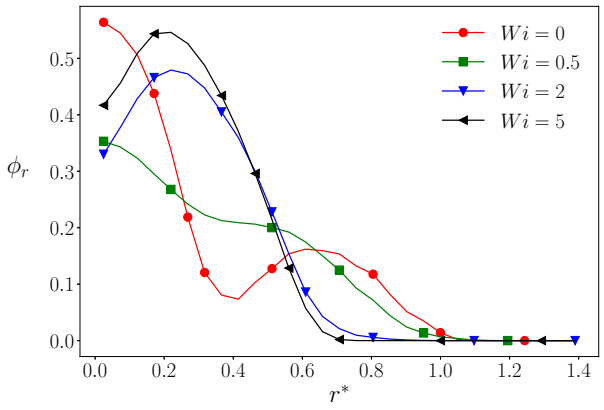

Fig. 15: Radial volume fraction of cells for $\phi = 10\%$, $\frac{a}{W} = 0.3$ and $Re = 37.8$

constant pressure-gradient at $\phi = 10\%$, $\frac{a}{W} = 0.3$ and $Re = 37.8$ and is plotted in Fig. 16(a). Our results show that the volumetric flow rate increases with increasing Wi number. In order to elaborate this effect, the velocity profile of the corresponding cases in the channel cross-section is plotted in Fig. 16(b). As Wi number increases, the velocity at centerline ($r^* = 0$) increases and the velocity profile becomes flatter in the central region. Therefore, the change in the velocity distribution across the microchannel due to the change in fluid elasticity results in the enhanced sample throughput in microfluidic devices. Furthermore, Fig. 16(a) shows that there is a critical Wi_c number above which the volumetric flow rate reaches a plateau. This change is attributed to the accumulation of cells in the core region where cells cannot be more compact above the critical Wi_c number. Besides, the effect of Reynolds number on the performance of the microfluidic devices in presence of polymeric fluids is investigated. The quasi-steady cell distance is plotted for various Re numbers at $\phi = 10\%$, $La = 500$ and $Wi = 2$ in Fig. 17. As it is shown, the distance of the cells from the centerline increases with increasing the Re number. This finding is in agreement with previous studies [34, 47] in which the dynamics of an isolated solid and deformable particle were studied in a microchannel. This behavior can be elaborated according to the strong dependence of inertial and elastic forces on Re number. The interaction between various forces such as inertial and elastic forces determines the final position of cells in the microchannel. The inertial effect is the dominant factor when $Re \gg Wi$ and the cells are expected to be driven toward the walls, while for the case with $Wi \gg Re$ the elastic force becomes dominant and the cells tend to accumulate in the central region of the microchannel.

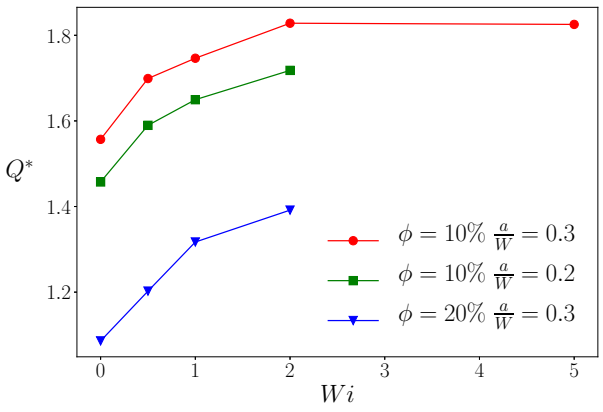

(a)

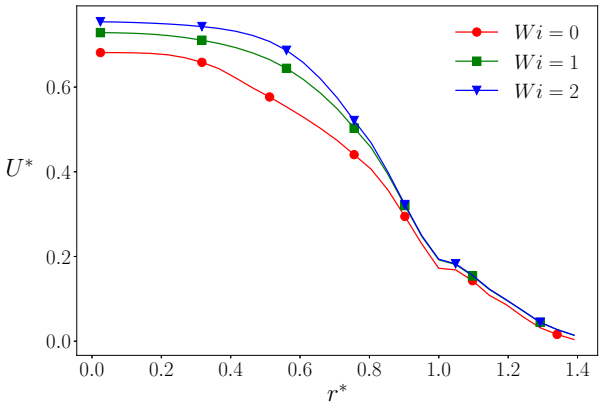

(b)

Fig. 16: (a) Volumetric flow rate of suspension for various Wi numbers at $Re = 37.8$ and (b) the velocity profile at $\phi = 10\%$, $La = 500$, $\frac{a}{W} = 0.3$ and $Re = 37.8$

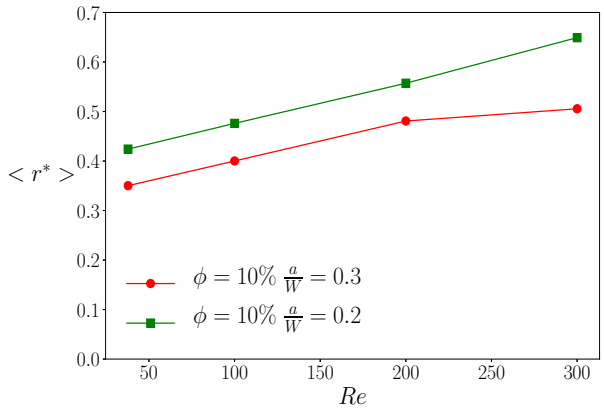

Fig. 17: Quasi-steady cell distance for various Re numbers at $\phi = 10\%$, $La = 500$ and $Wi = 2$

4 Conclusions

In this work, the dynamics of a cell suspension flowing in Newtonian and viscoelastic fluids is investigated. We study the effect of the cell size ($\frac{a}{W}$), cell volume fraction (ϕ), inertia (Re), deformability (La) and fluid elasticity (Wi) on the motion of cell suspension and the performance of the microfluidic devices composed of a straight microchannel. The variation of the aforementioned factors modulates the governing forces and influences the distribution of cells in the microchannel. Our results show that increasing the La number leads to the increase in the cell distance from the channel centerline (r^*) and reduction in the volumetric flow rate of the exiting flow (Q^*). These variables are also affected by the cell size and cell volume fraction. Increasing the cell size pushes the cells further toward the wall and this effect can be reinforced by increasing the cell volume fraction. However, the increase in $\frac{a}{W}$ and ϕ has an opposite effect on the volumetric flow rate and causes the decrease in Q^*. Our findings suggest that adding a polymer in suspending fluid pushes the cells further toward the centerline compared to a Newtonian fluid and can be used in devices that require centerline focusing of the cells such as cytometers. It is shown that increasing fluid elasticity (Wi) yields the reduction in cell distance from the centerline, while it increases the volumetric flow rate of the exiting flow. Furthermore, the effect of the inertia (Re) is investigated for both Newtonian and viscoelastic fluids. The results indicate that the change in the Reynolds number does not significantly affect the suspension dynamics, while an opposite behavior is observed in a viscoelastic fluid in which the cells are driven further toward the wall due to increase in the inertial effects.

A Acknowledgement

This research was partially supported by a grant from National Science Foundation [CBET-1705371].

B Conflicts of interest

There are no conflicts of interest to declare.

C Appendix

In order to check the mesh and the domain size independency of the computational results, we follow the method used in Doddi *et. al* [15] where the volumetric flow rate of the flow is investigated for various grid and domain sizes. Figure 18.(a) shows the volumetric flow rate of the cell suspension in a Newtonian fluid at $Re = 100$, $\phi = 10\%$ and $\frac{a}{W} = 0.3$ for various La numbers with $128 \times 76 \times 76$ and $200 \times 133 \times 133$ grid points in x, y and z directions, respectively. The maximum error between two different grid sizes is 2.44%. Hence, our results indicate that the numerical simulation performed in this study is independent of the mesh sizes. The results for the domain independency of the simulation is also plotted

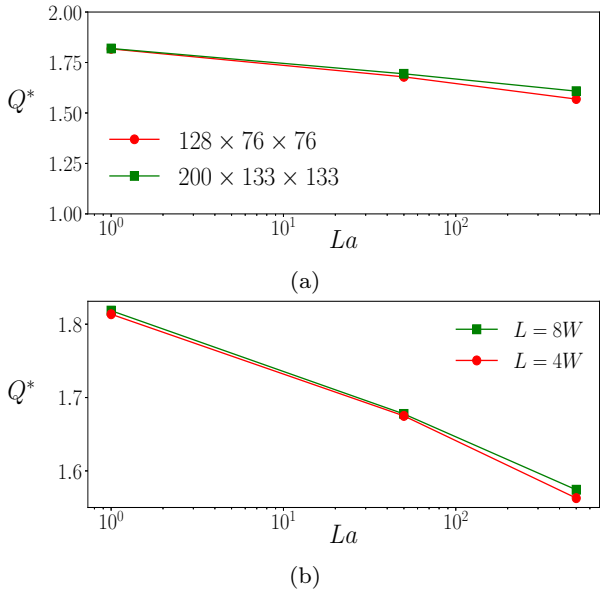

Fig. 18: The volumetric flow rate at $Re = 100$, $\phi = 10\%$ and $\frac{a}{W} = 0.3$ (a) for $128 \times 76 \times 76$ and $200 \times 133 \times 133$ grid points and (b) for $L_x = 4W$ and $8W$ in x direction

in Fig. 18(b) . The variation of the volumetric flow rate at $Re = 100$, $\phi = 10\%$ and $\frac{a}{W} = 0.3$ for two different domain sizes ($L_x = 4W$ and $8W$) in the x direction along which the periodic boundary condition is considered. The maximum error between two channel geometries is 0.71% that proves the independency of the numerical results against the computational domain size.

References

1. Asmolov, E. S. (1999). The inertial lift on a spherical particle in a plane poiseuille flow at large channel reynolds number. *Journal of Fluid Mechanics*, 381:63–87.
2. Chang, K.-S. and Olbricht, W. L. (1993). Experimental studies of the deformation and breakup of a synthetic capsule in steady and unsteady simple shear flow. *Journal of Fluid Mechanics*, 250:609–633.
3. Charrier, J., Shrivastava, S., and Wu, R. (1989). Free and constrained inflation of elastic membranes in relation to thermoforming—non-axisymmetric problems. *The Journal of Strain Analysis for Engineering Design*, 24(2):55–74.
4. Choi, Y.-S., Seo, K.-W., and Lee, S.-J. (2011). Lateral and cross-lateral focusing of spherical particles in a square microchannel. *Lab on a Chip*, 11(3):460–465.
5. Chorin, A. J. (1968). Numerical solution of the navier-stokes equations. *Mathematics of computation*, 22(104):745–762.
6. Chung, T. D. and Kim, H. C. (2007). Recent advances in miniaturized microfluidic flow cytometry for clinical use. *Electrophoresis*, 28(24):4511–4520.
7. Cooley, M., Sarode, A., Hoore, M., Fedosov, D. A., Mitragotri, S., and Gupta, A. S. (2018). Influence of particle size and shape on their margination and wall-adhesion: implications in drug delivery vehicle design across nano-to-micro scale. *Nanoscale*, 10(32):15350–15364.
8. D'Avino, G., Greco, F., and Maffettone, P. L. (2017). Particle migration due to viscoelasticity of the suspending liquid and its relevance in microfluidic devices. *Annual Review of Fluid Mechanics*, 49:341–360.
9. D'Avino, G., Romeo, G., Villone, M. M., Greco, F., Netti, P. A., and Maffettone, P. L. (2012). Single line particle focusing induced by viscoelasticity of the suspending liquid: theory, experiments and simulations to design a micropipe flow-focuser. *Lab on a Chip*, 12(9):1638–1645.
10. Del Giudice, F., D'Avino, G., Greco, F., Netti, P. A., and Maffettone, P. L. (2015). Effect of fluid rheology on particle migration in a square-shaped microchannel. *Microfluidics and Nanofluidics*, 19(1):95–104.
11. Del Giudice, F., Sathish, S., D'Avino, G., and Shen, A. Q. (2017). "from the edge to the center": viscoelastic migration of particles and cells in a strongly shear-thinning liquid flowing in a microchannel. *Analytical chemistry*.
12. Di Carlo, D. (2009). Inertial microfluidics. *Lab on a Chip*, 9(21):3038–3046.
13. Di Carlo, D., Edd, J. F., Humphry, K. J., Stone, H. A., and Toner, M. (2009). Particle segregation and dynamics in confined flows. *Physical review letters*, 102(9):094503.
14. Di Carlo, D., Irimia, D., Tompkins, R. G., and Toner, M. (2007). Continuous inertial focusing, ordering, and separation of particles in microchannels. *Proceedings of the National Academy of Sciences*, 104(48):18892–18897.
15. Doddi, S. K. and Bagchi, P. (2009). Three-dimensional computational modeling of multiple deformable cells flowing in microvessels. *Physical Review E*, 79(4):046318.
16. Faridi, M. A., Ramachandraiah, H., Banerjee, I., Ardabili, S., Zelenin, S., and Russom, A. (2017). Elasto-inertial microfluidics for bacteria separation from whole blood for sepsis diagnostics. *Journal of nanobiotechnology*, 15(1):3.
17. Fedosov, D. A., Caswell, B., Popel, A. S., and Karniadakis, G. E. (2010). Blood flow and cell-free layer in microvessels. *Microcirculation*, 17(8):615–628.
18. Feng, J., Hu, H. H., and Joseph, D. D. (1994). Direct simulation of initial value problems for the motion of solid bodies in a newtonian fluid part 1. sedimentation. *Journal of Fluid Mechanics*, 261:95–134.
19. Friend, J. and Yeo, L. Y. (2011). Microscale acoustofluidics: Microfluidics driven via acoustics and ultrasonics. *Reviews of Modern Physics*, 83(2):647.
20. Godin, J., Chen, C.-H., Cho, S. H., Qiao, W., Tsai, F., and Lo, Y.-H. (2008). Microfluidics and photonics for bio-system-on-a-chip: A review of advancements in technology towards a microfluidic flow cytometry chip. *Journal of biophotonics*, 1(5):355–376.
21. Gossett, D. R., Weaver, W. M., Mach, A. J., Hur, S. C., Tse, H. T. K., Lee, W., Amini, H., and Di Carlo, D. (2010). Label-free cell separation and sorting in microfluidic systems. *Analytical and bioanalytical chemistry*, 397(8):3249–3267.
22. Ho, B. and Leal, L. (1974). Inertial migration of rigid spheres in two-dimensional unidirectional flows. *Journal of fluid mechanics*, 65(2):365–400.
23. Howell Jr, P. B., Golden, J. P., Hilliard, L. R., Erickson, J. S., Mott, D. R., and Ligler, F. S. (2008). Two simple and rugged designs for creating microfluidic sheath flow. *Lab on a Chip*, 8(7):1097–1103.
24. Hur, S. C., Tse, H. T. K., and Di Carlo, D. (2010). Sheathless inertial cell ordering for extreme throughput flow cytometry. *Lab on a Chip*, 10(3):274–280.
25. Karimi, A., Yazdi, S., and Ardekani, A. (2013). Hydrodynamic mechanisms of cell and particle trapping in microfluidics. *Biomicrofluidics*, 7(2):021501.

26. Karnis, A., Goldsmith, H., and Mason, S. (1966). The flow of suspensions through tubes: V. inertial effects. *The Canadian Journal of Chemical Engineering*, 44(4):181–193.
27. Kilimnik, A., Mao, W., and Alexeev, A. (2011). Inertial migration of deformable capsules in channel flow. *Physics of fluids*, 23(12):123302.
28. Krüger, T., Kaoui, B., and Harting, J. (2014). Interplay of inertia and deformability on rheological properties of a suspension of capsules. *Journal of Fluid Mechanics*, 751:725–745.
29. Kunze, A., Che, J., Karimi, A., and Di Carlo, D. (2015). Research highlights: cell separation at the bench and beyond. *Lab on a Chip*, 15(3):605–609.
30. Lancaster, C., Kokoris, M., Nabavi, M., Clemmens, J., Maloney, P., Capadanno, J., Gerdes, J., and Battrell, C. (2005). Rare cancer cell analyzer for whole blood applications: Microcytometer cell counting and sorting subcircuits. *Methods*, 37(1):120–127.
31. Lee, D. J., Brenner, H., Youn, J. R., and Song, Y. S. (2013). Multiplex particle focusing via hydrodynamic force in viscoelastic fluids. *Scientific reports*, 3.
32. Leonard, B. P. (1979). A stable and accurate convective modelling procedure based on quadratic upstream interpolation. *Computer methods in applied mechanics and engineering*, 19(1):59–98.
33. Leshansky, A., Bransky, A., Korin, N., and Dinnar, U. (2007). Tunable nonlinear viscoelastic "focusing" in a microfluidic device. *Physical review letters*, 98(23):234501.
34. Li, G., McKinley, G. H., and Ardekani, A. M. (2015). Dynamics of particle migration in channel flow of viscoelastic fluids. *Journal of Fluid Mechanics*, 785:486–505.
35. Li, X. and Pozrikidis, C. (2000). Wall-bounded shear flow and channel flow of suspensions of liquid drops. *International journal of multiphase flow*, 26(8):1247–1279.
36. Lim, E. J., Ober, T. J., Edd, J. F., Desai, S. P., Neal, D., Bong, K. W., Doyle, P. S., McKinley, G. H., and Toner, M. (2014). Inertio-elastic focusing of bioparticles in microchannels at high throughput. *Nature communications*, 5.
37. Liu, C., Xue, C., Chen, X., Shan, L., Tian, Y., and Hu, G. (2015). Size-based separation of particles and cells utilizing viscoelastic effects in straight microchannels. *Analytical chemistry*, 87(12):6041–6048.
38. Lu, X., Liu, C., Hu, G., and Xuan, X. (2017). Particle manipulations in non-newtonian microfluidics: A review. *Journal of Colloid and Interface Science*.
39. Nam, J., Tan, J. K. S., Khoo, B. L., Namgung, B., Leo, H. L., Lim, C. T., and Kim, S. (2015). Hybrid capillary-inserted microfluidic device for sheathless particle focusing and separation in viscoelastic flow. *Biomicrofluidics*, 9(6):064117.
40. Paiè, P., Bragheri, F., Di Carlo, D., and Osellame, R. (2017). Particle focusing by 3d inertial microfluidics. *Microsystems & Nanoengineering*, 3:17027.
41. Pamme, N. (2006). Magnetism and microfluidics. *Lab on a Chip*, 6(1):24–38.
42. Pethig, R. (2010). Dielectrophoresis: Status of the theory, technology, and applications. *Biomicrofluidics*, 4(2):022811.
43. Popel, A. S. and Johnson, P. C. (2005). Microcirculation and hemorheology. *Annu. Rev. Fluid Mech.*, 37:43–69.
44. Pozrikidis, C. (2003). *Modeling and simulation of capsules and biological cells*. CRC Press.
45. Pranay, P., Henríquez-Rivera, R. G., and Graham, M. D. (2012). Depletion layer formation in suspensions of elastic capsules in newtonian and viscoelastic fluids. *Physics of Fluids*, 24(6):061902.
46. Raffiee, A. H., Dabiri, S., and Ardekani, A. M. (2017a). Deformation and buckling of microcapsules in a viscoelastic matrix. *Physical Review E*, 96(3):032603.
47. Raffiee, A. H., Dabiri, S., and Ardekani, A. M. (2017b). Elasto-inertial migration of deformable capsules in a microchannel. *Biomicrofluidics*, 11(6):064113.
48. Ramanujan, S. and Pozrikidis, C. (1998). Deformation of liquid capsules enclosed by elastic membranes in simple shear flow: large deformations and the effect of fluid viscosities. *Journal of Fluid Mechanics*, 361:117–143.
49. Romeo, G., D'Avino, G., Greco, F., Netti, P. A., and Maffettone, P. L. (2013). Viscoelastic flow-focusing in microchannels: scaling properties of the particle radial distributions. *Lab on a Chip*, 13(14):2802–2807.
50. Schaaf, C. and Stark, H. (2017). Inertial migration and axial control of deformable capsules. *Soft Matter*.
51. Schonberg, J. A. and Hinch, E. (1989). Inertial migration of a sphere in poiseuille flow. *Journal of Fluid Mechanics*, 203:517–524.
52. Segre, G. (1961). Radial particle displacements in poiseuille flow of suspensions. *Nature*, 189:209–210.
53. Seo, K. W., Kang, Y. J., and Lee, S. J. (2014). Lateral migration and focusing of microspheres in a microchannel flow of viscoelastic fluids. *Physics of Fluids*, 26(6):063301.
54. Sethu, P., Sin, A., and Toner, M. (2006). Microfluidic diffusive filter for apheresis (leukapheresis). *Lab on a Chip*, 6(1):83–89.
55. Skalak, R., Tozeren, A., Zarda, R., and Chien, S. (1973). Strain energy function of red blood cell membranes. *Biophysical Journal*, 13(3):245–264.
56. Sundararajan, N., Pio, M. S., Lee, L. P., and Berlin, A. A. (2004). Three-dimensional hydrodynamic focusing in polydimethylsiloxane (pdms) microchannels. *Journal of Microelectromechanical systems*, 13(4):559–567.
57. Unverdi, S. O. and Tryggvason, G. (1992). A front-tracking method for viscous, incompressible, multi-fluid flows. *Journal of computational physics*, 100(1):25–37.
58. van de Stolpe, A., Pantel, K., Sleijfer, S., Terstappen, L. W., and Den Toonder, J. M. (2011). Circulating tumor cell isolation and diagnostics: toward routine clinical use.
59. Villone, M., D'Avino, G., Hulsen, M., Greco, F., and Maffettone, P. (2013). Particle motion in square channel flow of a viscoelastic liquid: Migration vs. secondary flows. *Journal of Non-Newtonian Fluid Mechanics*, 195:1–8.
60. Yang, S., Kim, J. Y., Lee, S. J., Lee, S. S., and Kim, J. M. (2011). Sheathless elasto-inertial particle focusing and continuous separation in a straight rectangular microchannel. *Lab on a Chip*, 11(2):266–273.
61. Zeng, L., Balachandar, S., and Fischer, P. (2005). Wall-induced forces on a rigid sphere at finite reynolds number. *Journal of Fluid Mechanics*, 536:1–25.
62. Zhao, H., Shaqfeh, E. S., and Narsimhan, V. (2012). Shear-induced particle migration and margination in a cellular suspension. *Physics of Fluids*, 24(1):011902.